Magic-Angle Spinning Nuclear Magnetic Resonance under Ultrahigh Field Reveals Two Forms of Intermolecular Interaction within CH_2Cl_2-Treated (3^1R)-Type Bacteriochlorophyll *c* Solid Aggregate

Mitsuo Umetsu,[†,‡] Johan G. Hollander,[†] Jörg Matysik,[†] Zheng-Yu Wang,[§] Tadafumi Adschiri,[‡] Tsunenori Nozawa,[§] and Huub J. M. de Groot*[,†]

Leiden Institute of Chemistry, Gorlaeus Laboratories, Leiden University, PO Box 9502, 2300 RA Leiden, The Netherlands, Institute of Multidisciplinary Research for Advanced Materials, Tohoku University, 2-1-1, Katahira, Aoba-ku, Sendai, 980-8577, Japan, and Department of Biomolecular Engineering, Graduate School of Engineering, Tohoku University, Aobayama 07, Aoba-ku, Sendai 980-8579, Japan

Received: April 10, 2003; In Final Form: July 9, 2003

(3^1R)-bacteriochlorophyll (BChl) *c* solid aggregates with an absorbance around 740 nm were formed from BChl *c* dimers, and 2-D homonuclear $^{13}C-^{13}C$ radio frequency-driven dipolar recoupling as well as proton-driven spin diffusion dipolar correlation NMR spectra have been collected in ultrahigh magnetic field. Doubling of signals is observed for most carbons in the BChl *c* macrocycle, leading to two correlation networks. In this way, two major fractions denoted types A and B are identified. Some of the ring carbons show multiple resonances, revealing additional slight differences in microstructural environment. 2-D heteronuclear $^1H-^{13}C$ correlation data have been recorded using the frequency- and phase-switched Lee−Goldburg technique to assign the ^1H response. ^{15}N chemical shifts are assigned from 2-D heteronuclear $^{15}N-^{13}C$ correlation experiments using spectrally induced filtering in combination with cross polarization. Also the nitrogen atoms in the pyrrole rings I, II, and IV (N_I, N_{II}, and N_{IV}, respectively) show two sets of resonances, each of which is connected to a single ^{13}C correlation network A or B. The ^{13}C chemical shifts are compared with the signals from antiparallel dimers in solution and with the response from chlorosomes previously reported. The data clearly show that the stacking in CH_2Cl_2-treated aggregates is different from the stacking in the chlorosomes and hexane-treated aggregates. Some degree of similarity with the antiparallel dimer form in solution transpires, in particular for the type A species. It is proposed that the CH_2Cl_2 precipitate represents a structural intermediate between the antiparallel dimer and the parallel stack as found in the chlorosome.

Introduction

The chlorosome is a light-harvesting entity in the green sulfur and filamentous photosynthetic bacteria that contains bacteriochlorophyll (BChl) *c* and *d* or *e* in some species as a major pigment component.[1] The chlorosome antennae are attached to the cytoplasmic side of the inner cell membrane, and monogalactosyldiglycerol (MGDG) is considered to form a monolayer on the surface of the chlorosome.[2−5] Inside the MGDG envelope, a large amount of BChl *c* forms rodlike aggregates called "rod elements".[2,3]

The Q_y transition of monomeric BChl *c* in hydrophilic solvents appears at ∼660−670 nm, while the transition in the chlorosome is redshifted to ∼740−750 nm.[6,7] To elucidate the electronic mechanism of this redshift for BChl *c* in vivo has been one of the major topics in recent studies of chlorosome antennae. At an early stage, several pigment−protein interaction models have been proposed since a minor protein fraction was isolated from chlorosomes.[8−10] However, it was recently reported that pure BChl *c* can form aggregates in nonpolar solvents that resemble those of native chlorosome.[11−13] For *Chloroflexus aurantiacus* and *Chlorobium tepidum* and *limicola*, protein-free chlorosomes were reconstituted in aqueous solutions,[14−16] while Uehara et al. reported that the oligomers formed by BChl *c* in the presence of MGDG show spectroscopic properties that are similar to those of native chlorosomes.[17] These results provide convincing evidence that proteins do not directly mediate the organization of BChl *c* in the chlorosome, and self-aggregation of BChl *c* plays a predominant role in the chlorosome. Hence, elucidating the mechanism of self-aggregation is generally considered essential for understanding the chlorosome structure, but also the aggregation behavior is expected to be a good model for in vivo self-assembly of macromolecule in terms of the field of physical chemistry.

BChl *c* has the same chlorin ring as chlorophyll (Chl) *a*. Its characteristic hydroxyl group at the 3^1 position enables the self-aggregation of BChl *c*. It is well known that high aggregates with a Q_y absorption maximum around 740 nm can be formed from only BChl *c* in hexane and cyclohexane, but the aggregation behavior and the properties of the electronic transition depend on the ratios of the various homologues of BChl *c*.[17] Complementing to high aggregates, (3^1R)-type BChl *c* with a *R*-type chiral center at the 3^1 position can form two kinds of small oligomeric aggregates in CH_2Cl_2, $CHCl_3$, CCl_4, and benzene with absorption maxima at 680 and 703−710 nm.[18,19]

For the small aggregates, it has been demonstrated on the basis of small-angle neutron scattering (SANS) and ^1H, ^{13}C,

* Author to whom correspondence may be addressed. Tel: +31-71-5274539. Fax: +31-71-5274603. E-mail: ssnmr@chem.leidenuniv.nl.
† Leiden University.
‡ Institute of Multidisciplinary Research for Advanced Materials, Tohoku University.
§ Department of Biomolecular Engineering, Tohoku University.

10.1021/jp034957a CCC: $27.50
Published on Web 01/30/2004

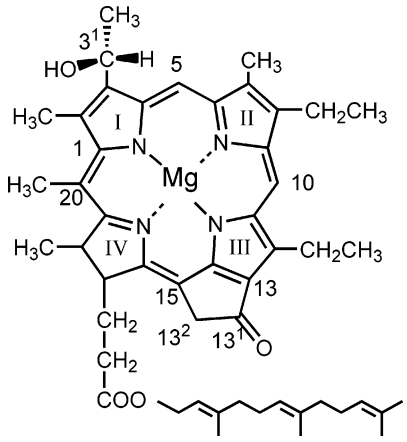

Figure 1. Molecular structure of the (3^1R)-[*E*,*E*]BChl c_F.

and ^{15}N NMR experiments that the 710 nm rich species of (3^1R)-BChl *c* in neat CCl_4 predominately consists of dimers with an antiparallel piggy-back conformation.[20−22] Recent circular and magnetic circular dichroism (CD and MCD) studies have been interpreted in terms of two types of BChl *c* dimers with different conformations: an antiparallel dimer with two $Q_y(0-0)$ exciton components at 680 and 710 nm and a transient dimer with a single $Q_y(0-0)$ transition at 680 nm.[23] In contrast, (3^1S)-BChl *c* forms large aggregates with a Q_y absorption maximum at ∼740−750 nm directly from the monomeric form in CH_2Cl_2, $CHCl_3$, or CCl_4 instead of the small intermediates, and further, (3^1S)-BChl *c* high aggregate in vitro structurally resembles the native chlorosome, despite the fact that (3^1R)-BChl *c* is more abundant than (3^1S)-BChl *c* in the chlorosome.[24−26] The influence of (3^1S)-BChl *c* on the aggregation behavior of (3^1R)-BChl *c* is of importance for understanding the self-aggregation in the chlorosome;[27,28] however, the exact mechanism of the self-aggregation and the aggregate structure for (3^1R)-BChl *c* has not yet been solved.

The difficulties for elucidating the formation mechanism to the high aggregate is due to a phase transition from soluble form (monomer and dimers) to solid state (high aggregate) and the structural inhomogeneity of the high aggregates. For the high aggregate formed in hexane from a mixture of various BChl *c* homologues, solid-state cross polarization/magic-angle spinning (CP/MAS) ^{13}C NMR spectra have been measured because the hexane-treated aggregates show no X-ray diffraction,[29] and these data reveal a close structural similarity between the high aggregate and the ordered BChl *c* in the chlorosome. The CP/MAS data of the hexane-treated aggregate and the chlorosome are similarly broadened due to structural inhomogeneity. Recently, 2-D homonuclear ($^{13}C-^{13}C$) dipolar correlation spectroscopy was applied to the BChl *c* solid aggregates formed in hexane and to the native chlorosome in order to assign the carbon resonances.[13,30] In addition, the proton resonances were carefully assigned by heteronuclear 2-D and 3-D correlation spectra.[30,31]

In the present study, we have focused on the 2-D solid-state NMR experiments of the solid aggregate prepared from a homologue of (3^1R)-BChl *c* with ethyl groups at the 8 and 12 positions and farnesyl as the ester chain ((3^1R)-[E,E]BChl c_F, Figure 1). About 50% of the BChl *c* homologues in the chlorosome of *Chlorobium tepidum* is the (3^1R)-[*E*,*E*]BChl c_F, which is the most abundant component.[13,32] Elucidating the aggregate structure and self-organization process of the (3^1R)-[*E*,*E*]BChl c_F can supply a significant hint for understanding the construction of chlorosome and the affect of various BChl *c* homologues on the aggregation behavior of the abundant (3^1R)-BChl *c*, which also would give a control system for self-assembly of the macromolecule. The formation of the aggregate prepared by drying a solution of (3^1R)-[*E*,*E*]BChl c_F in CH_2Cl_2 has been traced by time-resolved multichannel optical spectroscopy.[33] Throughout the drying, the solid aggregate with an absorbance around 740 nm is formed through an antiparallel and a transient dimer.[23,33] In this report, the coexistence of two different structures in the solid aggregates formed from the dimers is clearly demonstrated from 2-D homonuclear ($^{13}C-^{13}C$) and heteronuclear ($^1H-^{13}C$ and $^{15}N-^{13}C$) NMR spectra. The ^{13}C chemical shifts suggest that the CH_2Cl_2 precipitate represents a structural intermediate between the antiparallel dimer and the parallel stack as found in the chlorosome. The presence of antiparallel dimers in solution leads to a solid aggregate that is different from the structure in the native chlorosme.

Experimental Section

Materials and Sample Preparation. (3^1R)-[*E*,*E*]BChl c_F was extracted with methanol from *Chlorobium tepidum* dry cells and purified by a reverse-phase HPLC column (TOSOH TSKgel ODS-80Ts) with the same method as previously reported.[34] For the preparation of natural abundance BChl *c*, cells were grown in a medium containing sodium bicarbonate, ammonium acetate, and ammonium chloride as carbon and nitrogen sources.[34] For the ^{13}C- and ^{15}N-labeled BChl *c*, the ammonium acetate was not used and the concentrations of sodium bicarbonate and ammonium chloride were adjusted to balance the carbon and nitrogen weights in the media. All the carbons in BChl *c* were uniformly ^{13}C labeled with $NaH^{13}CO_3$ (^{13}C >98% atom, Isotec Inc.) as the sole carbon source, and $^{15}NH_4Cl$ (^{15}N >99% atom, Isotec Inc.) was applied for uniformly ^{15}N-labeled BChl *c*.[22] For MAS NMR measurements, the $^{13}C-^{15}N$-labeled (3^1R)-[*E*,*E*]-BChl c_F (about 20 mg) was dissolved in neat CH_2Cl_2 treated with Na_2CO_3, and then the BChl $c-CH_2Cl_2$ solution was dried spontaneously in a 4-mm rotor under dry air and vacuum. The residue in the rotor after complete evaporation of the solvent was measured.

NMR Measurements. MAS NMR spectra were collected at room temperature with a Bruker AV750 spectrometer equipped with a 4-mm triple resonance probe. MAS frequencies of 10−13 kHz were used and were kept stable within a few Hz. In all solid-state NMR experiments, two-pulse phase modulation (TPPM) was used for proton decoupling with pulses of ∼7 μs alternating between two phases separated by an angle of 15°.[35] A CP sequence with a linear ramp from 100−50% was applied for the heteronuclear $^1H-^{13}C$ polarization transfer at high MAS rates during the CP time of 4 ms.[36] The 2-D radio frequency-driven dipolar recoupling (RFDR) homonuclear $^{13}C-^{13}C$ dipolar correlation spectra were measured with an XY-8 recoupling pulse sequence in the mixing period and acquired using time-proportional phase incrementation (TPPI) for simulated phase sensitive detection.[37] The 2-D proton-driven spin diffusion (PDSD) homonuclear $^{13}C-^{13}C$ dipolar correlation spectra were measured using spin-diffusion techniques[38] and collected with TPPI. The 2-D homonuclear ^{13}C spectra were acquired with a radio frequency (rf) of 188.6 MHz and collected in 256 t_1 points, with 1024 data points in t_2. Scans (256) were collected for each t_1 point using a repetition time of 1 s. The 2-D heteronuclear $^1H-^{13}C$ correlation spectra were measured with FS-LG and ramp-CP sequences on the ^1H rf field as described previously.[39] The phases of the entire FS-LG sequence and the two magic-angle pulses are varied in a TPPI scheme in order to simulate phase-sensitive detection. The contact time for the CP was

limited to 500 μs in order to avoid homonuclear spin-diffusion-type processes in both proton and labeled-carbon spin reservoirs. The spectra were collected with 256 t_1 and 1200 t_2 data points using a repetition time of 1 s. $^{15}N-^{13}C$ correlation spectra were measured with the pulse sequence of spectrally induced filtering in combination with CP (SPECIFIC-CP).[40−42] ^1H polarization was first transferred to ^{13}C matching with a 100%/70% linear ramp on the ^1H rf field during 2 ms. After the first transfer to ^{13}C, ^{15}N polarization was created by the SPECIFIC-CP transfer during 5.1 ms. t_1 (128) and t_2 (1024) data points were recorded with 3072 scans for each t_1 point using a repetition time of 2 s.

Results

Figure 2 shows a contour plot of a 2-D CP/MAS homonuclear $^{13}C-^{13}C$ RFDR dipolar correlation NMR spectrum recorded in a magnetic field of 17.6 T from the CH_2Cl_2-treated solid aggregates of uniformly ^{13}C-labeled (3^1R)-[*E*,*E*]BChl c_F. With the short mixing time $\tau_m = 2.7$ ms, many clear 2-D cross-peaks appear, revealing transfer of coherence between olefinic carbons in a macrocycle ring. To identify the spinning sideband signals in the spectra, we measured 2-D spectra with various MAS rotation rates (10, 12, and 13 kHz) at each magnetic field of 9.5 and 17.6 T. All carbons of the BChl *c* macrocycle, except 3^1-C, 10-C, 17^1-C, and 20^1-C, have at least two sets of resonances. From the global pattern of these responses, two different species of BChl *c* (types A and B, corresponding to the correlation networks A and B) can be recognized. Signals from the meso carbon 5-C are observed at 94.8 ppm and at 101.5 ppm, and each of these 5-C resonances makes a separately resolved correlation network with 3-C, 4-C, and 6-C responses (solid and dashed lines in Figure 2). Similarly, two sets of correlations for the 3-C reveal doubling of 1-C and 2-C signals, which is confirmed by correlations with the 2^1-C as well. On the opposite side of the BChl *c* ring system, a well-resolved doubling of signals is observed for 13-C, 14-C, 15-C, and 16-C from the cross peaks of 13-C/14-C, 14-C/15-C, and 14-C/16-C. Although the 19-C/20-C correlations cannot be recognized in Figure 2 because of overlap with a series of spinning sidebands, the 19-C resonances are confirmed at another MAS rotation frequency $\omega_r/2\pi = 13$ kHz, and both the 19-C and the 20-C show a doubled response in the correlation spectrum (Figure 3). For the 17^3-C carbonyl carbon, two resonances are identified from the correlations with $17^{1,2}$-C. However, we could not connect these signals with the A and B patterns, since the 17^1 and 17^2 were not doubled.

Some of the carbons in the chlorin ring and peripheral substituents show multiple resonances. For instance, the 7-C resonance in the network A shows two cross peaks with 7^1-C in the same network (solid line in Figure 3), and then the doubling of signal of the 7-C in the network A let us recognize two resonances of 8-C (data not shown). Multiple signals are also detected for 2^1-C, 3-C, 12-C, 12^1-C, and 18^1-C through correlations between paraffinic and olefinic carbons. In contrast with the chlorin ring and its substituents, the resonances for the ^{13}C in the farnesyl chain give rise to relatively broad cross-peaks and the signals of individual structural species are not resolved (Figure 3).

Table 1 lists the ^{13}C NMR assignments of the (3^1R)-[*E*,*E*] BChl c_F solid aggregates treated in CH_2Cl_2. The ^{13}C chemical shifts were basically assigned through the contour plots of 2-D RFDR dipolar correlation spectra with several τ_m. It was found that polarization transfer between aliphatic carbons was easier with straightforward spin-diffusion techniques than with RFDR, and therefore 2-D PDSD dipolar correlation spectra were used to confirm the assignments of the carbon signals from the ^{13}C in the farnesyl chain and the other substituents.

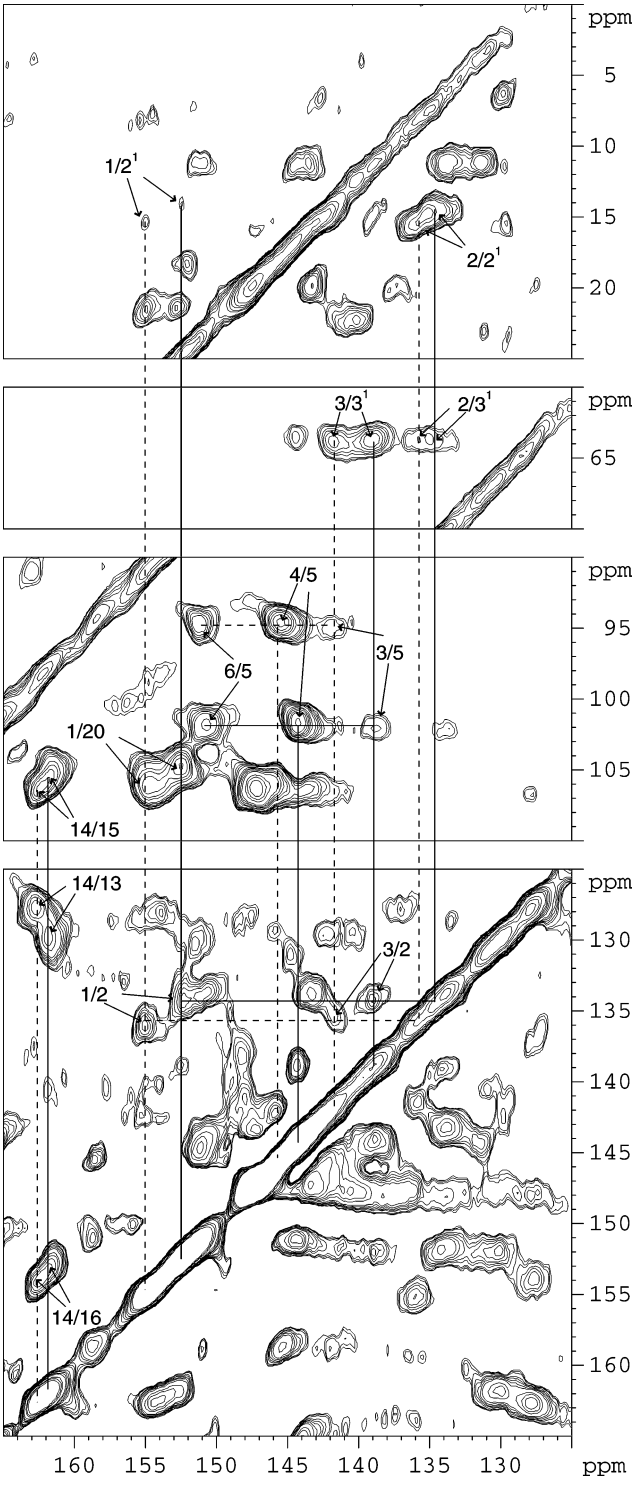

Figure 2. Contour plot of the 2-D CP/MAS RFDR $^{13}C-^{13}C$ dipolar correlation spectrum for the CH_2Cl_2-treated solid aggregate of uniformly ^{13}C-labeled (3^1R)-[*E*,*E*]BChl c_F in a magnetic field of 17.6 T. The MAS rotation frequency and the mixing time were 12 kHz and 2.7 ms, respectively. The numbering in the plot corresponds with Figure 1. The solid and dotted lines express the correlation networks A and B of carbon resonances, respectively.

Figure 4 shows a contour plot of a 2-D FS-LG decoupled heteronuclear $^1H-^{13}C$ dipolar correlation spectrum collected from the (3^1R)-[*E*,*E*]BChl c_F solid aggregate precipitated in CH_2Cl_2. FS-LG is an effective method for suppressing $^1H-^1H$ dipolar interactions at rapid MAS in high field.[39] With a spinning

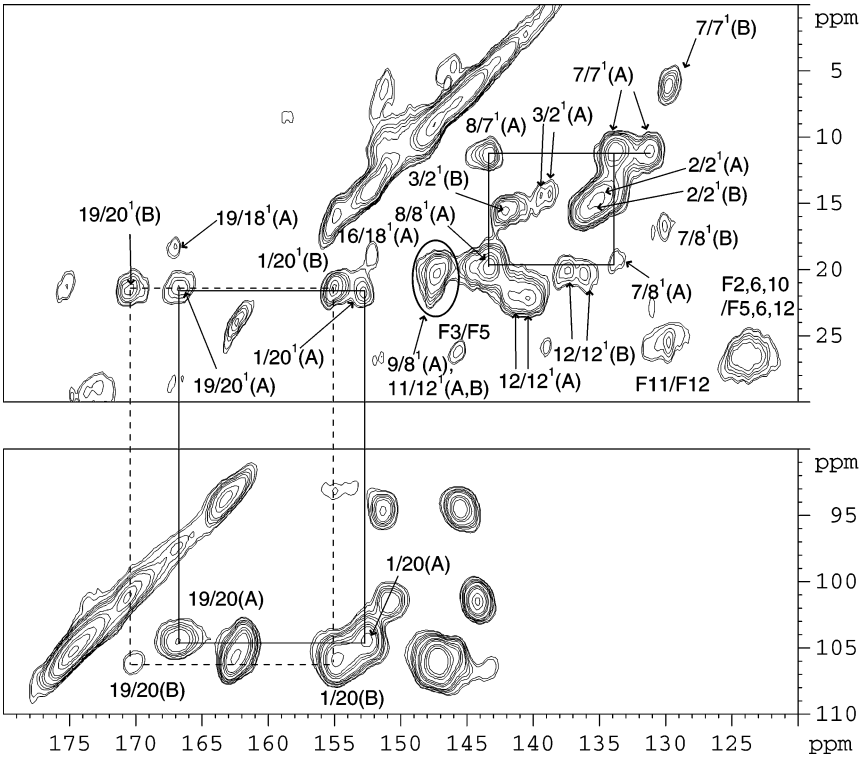

Figure 3. Contour plot of the 2-D RFDR $^{13}C-^{13}C$ correlation spectrum for the uniformly ^{13}C-labeled (3^1R)-[*E*,*E*]BChl c_F solid aggregate treated in CH_2Cl_2 in a magnetic field of 17.6 T. The MAS frequency and the mixing time were 13 kHz and 2.5 ms, respectively. The numbering in the plot corresponds with Figure 1. The cross peaks labeled with A and B are the dipole correlations in the networks A and B, respectively.

frequency of 12 kHz in the high magnetic field of 17.6 T, each of the two 5-C resonances makes an explicit correlation with 5-H responses at 7.5 and 7.9 ppm, respectively, revealing doubling of the 5-H signal. 3^1- and 3^2-H also have two signals from the correlations with the 5-C. In the 2-D $^1H-^{13}C$ correlation spectrum, doubling of signals for some protons is resolved and the proton resonances can be assigned to the two major correlation networks A and B identified for the ^{13}C response. A doubling of the 10-C response, which cannot be observed in homonuclear $^{13}C-^{13}C$ correlation spectra because of the small chemical shift difference, is well resolved with the heteronuclear $^1H-^{13}C$ correlation spectrum at high magnetic field. The 10-$^1H-^{13}C$ correlation peak doubling partially leads to two assignments for 10-C (105.8 and 106 ppm) and 10-H (9.1 and 10.6 ppm).

Figure 5 shows the 1-D CP/MAS ^{15}N NMR spectrum for the CH_2Cl_2-treated solid aggregate of uniformly $^{13}C-^{15}N$-labeled (3^1R)-BChl c_F in a magnetic field of 17.6 T. The N_{IV} position shows two broad resonances at 248 and 255 ppm with a substantial chemical-shift difference of 7 ppm, while sharp N_{II} signals are found with 208 ppm and 210 ppm chemical shifts. In the chemical shift region between 200 and 192 ppm, the spectrum is complicated. The N_I resonance in a monomer state is expected to appear around 200 ppm,[22] but only some weak signals are observed here. It is difficult to recognize the N_I resonance from the 1-D spectrum.

To assign the nitrogen response, a 2-D heteronuclear $^{15}N-^{13}C$ correlation spectrum has been measured using $^{15}N-^{13}C$ polarization transfer and the correlations between nitrogens and carbons directly attached to each other were detected (Figure 6). The two resonances of N_{IV} are correlated with their respective 16-C in the correlation networks A and B of carbon, revealing that the 248 ppm and 255 ppm signals belong to the networks A and B, respectively. The 210 ppm resonance of N_{II} makes an intense cross peak with 6-C and 9-C at 151 and 147.4 ppm in the network A, respectively, while another N_{II} resonance (208 ppm) is correlated with 6-C (151.5 ppm) and 9-C (146 ppm) in the network B. For N_I, we can distinguish the resonance from N_{III}, while the clear correlations of N_I with 1-C and 4-C in the networks A and B (at 197.7 and 195.7 ppm, respectively) lead to linking the N_I resonances with the correlation networks of the carbon. The 2-D $^{15}N-^{13}C$ correlation spectrum shows that each N_I, N_{II}, and N_{IV} has two sharp signals and that these can be linked with the correlation networks of the carbon. This supports the ^{13}C NMR result that two different major species of BChl *c* (types A and B) coexist in the CH_2Cl_2-treated solid aggregate. Around 200 ppm in the nitrogen field, weak and broad cross signals with 1-C and 4-C are observed, suggesting that the broad bands around 200 ppm in the 1-D ^{15}N spectrum are assigned to N_I. The weak signal of N_I is probably derived from a minor species different from the type A and B species.

Discussion

2-D correlation spectra are an effective tool for analyzing in detail polymorphisms arising from self-assembly of asymmetric molecules. The 2-D homonuclear $^{13}C-^{13}C$ RFDR and PDSD dipolar correlation NMR spectra provide two sets of resonances for most of the carbons in a chlorin ring and the peripheral substituents, and consequently, two different solid-state species (types A and B) can be identified in the CH_2Cl_2-treated solid aggregates of (3^1R)-[*E*,*E*]BChl c_F. This indicates the possibility that only the (3^1R)-[*E*,*E*]BChl c_F forms two different structures in the high aggregates. Figure 7 shows a schematic map of the ^{13}C chemical shift difference defined by $\Delta\delta = \delta_{solid} - \delta_{monomer}$ for each of the two species. The ^{13}C chemical shifts of the BChl *c* were referenced to the monomer state in the CD_3OD-added $CDCl_3$, which is thought to have a Mg coordination similar to the aggregated BChl *c*.[13] Significant upfield shifts >2 ppm are detected only for 2^1-C, 3-C, and 8^2-C in the type A solid state (Figure 7a), while in the type B solid state, there are upfield

TABLE 1: Assignments of ^{13}C Chemical Shifts of the (3^1R)-[*E*,*E*] BChl c_F in the Solid Aggregates Treated in CH_2Cl_2

	solid aggregates from CH_2Cl_2[a] (ppm)			
position	type A		type B	
13^1	196	(0.2)	196.8	(0.2)
17^3	(172.6 (1), 173.5(1))[b]			
19	167	(0.2)	170.5	(0.5)
14	161.9	(0.2)	163	(0.2)
16	152.4	(0.2)	154.5	(0.2)
1	152.2	(0.6)	155.5	(0.2)
6	150.9	(0.2)	151.5	(0.2)
11	148	(0.3)	148.2	(0.3)
9	147.4	(0.3)	146	(0.3)
3	139	(0.2)	141.8	(0.2)
	139.5	(0.2)		
4	144.2	(0.1)	145.8	(0.3)
8	143.6	(0.2)	142.2	(0.2)
	144.2	(0.2)		
F3	139 (0.3)			
12	140.5	(0.2)	136.3	(0.2)
	141.5	(0.4)	137.6	(0.2)
2	134.4	(0.2)	136	(0.2)
F7	134.5 (0.7)			
7	133.8	(0.3)	129.8	(0.1)
	131.4	(0.3)		
F11	130 (0.4)			
13	130	(0.2)	127.8	(0.2)
F10	124 (1)			
F6	124 (1)			
F2	119 (1)			
10	106.5[c] (0.2)			
15	105	(0.2)	106.5	(0.2)
20	104.5	(0.3)	106.2	(0.3)
5	101.5	(0.1)	94.8	(0.1)
3^1	64 (0.2)			
F1	61 (0.3)			
17	50.2	(0.5)	50.8	(0.5)
13^2	48	(0.4)	50	(0.4)
18	49	(0.3)	48	(0.3)
F8	39.5 (0.5)			
F4	39.5 (0.5)			
17^2	30 (0.8)			
17^1	30 (0.8)			
F9	26 (0.7)			
F5	26 (0.3)			
3^2	25.2	(0.3)	22.2	(0.3)
F12	26 (1)			
12^1	21.8	(0.3)	19.8	(0.3)
			20.2	(0.3)
20^1	21.5 (0.5)			
18^1	21	(0.5)	21	(0.5)
	18.5	(0.2)		
8^1	19.5	(0.2)	16.8	(0.2)
8^2	11.4	(0.2)	10.5	(0.2)
12^2	15	(0.2)	11.2	(0.2)
F11a	16.4 (0.8)			
2^1	14	(0.2)	15.8	(0.2)
	14.2	(0.2)		
F3a	15 (0.7)			
F7a	15 (0.7)			
7^1	11	(0.2)	6	(0.2)

[a] The estimated errors for the solid-state shifts are in parentheses. [b] The two signals for $C17^3$ could not be assigned to the type A or B species. [c] There are two signals for the 10-C in the 2-D $^1H-^{13}C$ correlation spectrum.

shifts >2 ppm for several carbons around pyrrole rings I, II, and III (Figure 7b). It has been reported that ring-current shifts due to the overlap of chlorin rings are the predominant factor causing the upfield shift of ^{13}C signals upon aggregation of Chl and BChl.[31,43,44] Thus, the ^{13}C shift maps presented in Figure 7 reveal the presence of two types of overlap of chlorin rings in the solid aggregate. In the type B solid state, the 19-C is shifted lowfield (Figure 7b). We consider at present that this is due to some polarization or skew effect of an unknown kind, since it is difficult to assign it to a positive ring-current shift.

A complete assignment of ^{13}C chemical shifts for the stable antiparallel dimer in CCl_4 has been reported,[22] while the homonuclear ($^{13}C-^{13}C$) and heteronuclear ($^1H-^{13}C$) correlation spectra have been measured for native chlorosomes.[13,31] The antiparallel dimer in CCl_4 has the "piggy-back" conformation, where the two 3^1-hydroxyl groups coordinate on the Mg atom of the other BChl *c*. This leads to a characteristic pattern of pronounced upfield shifts due to ring-current effects which is limited to carbons in or near ring I. In contrast, the NMR results for the native chlorosome show aggregation shifts for ring I and ring III, implying a parallel BChl *c* stack in which ring I of each BChl *c* molecule overlaps with ring III of the next one by the ligation of the 3^1-hydroxyl group to the Mg of the next molecule. The NMR spectra of the chlorosome also show two sets of carbon resonances for 4-C−9-C, 7^1-C, 19-C, and 20-C, suggesting two forms of parallel stacking, denoted by components I and II.[30,31] Associated upfield shifts are observed for the carbons around rings I and III for both components, while for the component II aggregation, shifts are present around ring II.[31]

For the CH_2Cl_2-treated solid aggregate of (3^1R)-[*E*,*E*]BChl c_F, the upfield shifts in the type A solid state are distributed around ring I, except for 8^2-C (Figure 7a), while the type B shifts are observed for the carbons attached to rings I, II, and III (Figure 7b). The upfield shift pattern of the type B solid state thus qualitatively resembles the component II in native chlorosome, while the pattern of the type A state is qualitatively similar to that of the antiparallel dimer in CCl_4. The analogy with the component II in the chlorosome is however not complete, since large upfield shifts are observed for 8^2-C and 12^2-C in the CH_2Cl_2-treated aggregates, which show no remarkable shift in the antiparallel dimer and native chlorosome. These shifts are probably due to the influence of multiple stacks in the structure. The ring-current effect from the adjacent stacks may be different between the type B solid species in the CH_2Cl_2-treated solid aggregate and the component II in native chlorosome.

In previous studies,[26,45] the calculation of the ring-current effects had been applied for several aggregate models BChl *c* can form; antiparallel dimer, the oligomers consisting of the antiparallel dimer, and the parallel BChl *c* stack structure. Similar to the comparison with the measured upfield shifts pattern for the antiparallel dimer and native chlorosome, the calculation results support that the upfield shifts pattern for the type A solid species is most suitable to the result of the antiparallel dimer while the upfield shifts pattern for the type *B* solid species is interpreted by the parallel BChl *c* stack structure rather than the oligomers consisting of the antiparallel dimer.[26,45] However, the upfield shifts at the 8-position in the type A solid species and around ring II in the type B solid species could not be explained by the calculation of the ring-current effects for the proposed aggregate models. This suggests that the upfield chemical shift around ring II is due to the influence of adjacent stacks in the aggregates.

Recently, evidence was found for the coexistence of two types of dimers, a stable antiparallel "closed" dimer (Figure 8a) and an unstable transient "open" dimer (Figure 8b), in (3^1R)-BChl $c-CH_2Cl_2$ solutions by a simultaneous deconvolution of absorption, CD and MCD spectra.[23] 2-D exchange spectroscopy (2-D EXSY) suggests that the polarity of the CD_2Cl_2 solvent accounts for the destabilization of the antiparallel dimer.[23] In addition, it

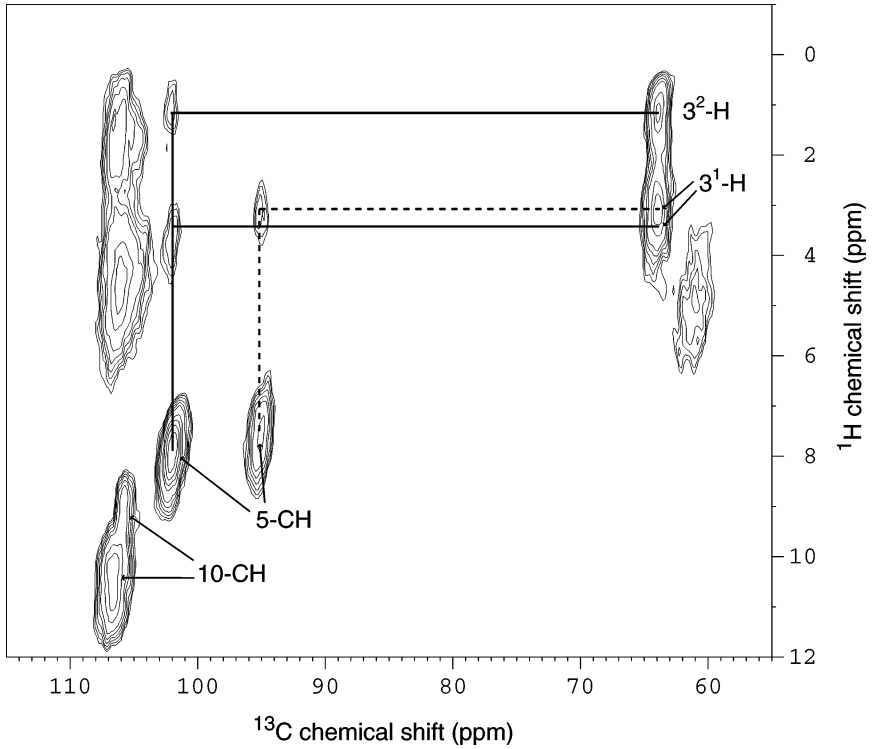

Figure 4. Contour plot of a 2-D heteronuclear $^{1}H-^{13}C$ FS-LG decoupled correlation spectrum for the uniformly ^{13}C-labeled (3^1R)-[*E*,*E*]BChl c_F solid aggregate treated in CH_2Cl_2. The magnetic field and MAS frequency were 17.6 T and 12 kHz, respectively, and the contact time for the $^{1}H-^{13}C$ polarization transfer was 500 μs. The lines indicate the correlation networks among 5-, 3^1-, and 3^2-H proton resonances and involving the 5-C carbon resonance. The solid and dashed lines are linked with the networks A and B of carbon, respectively.

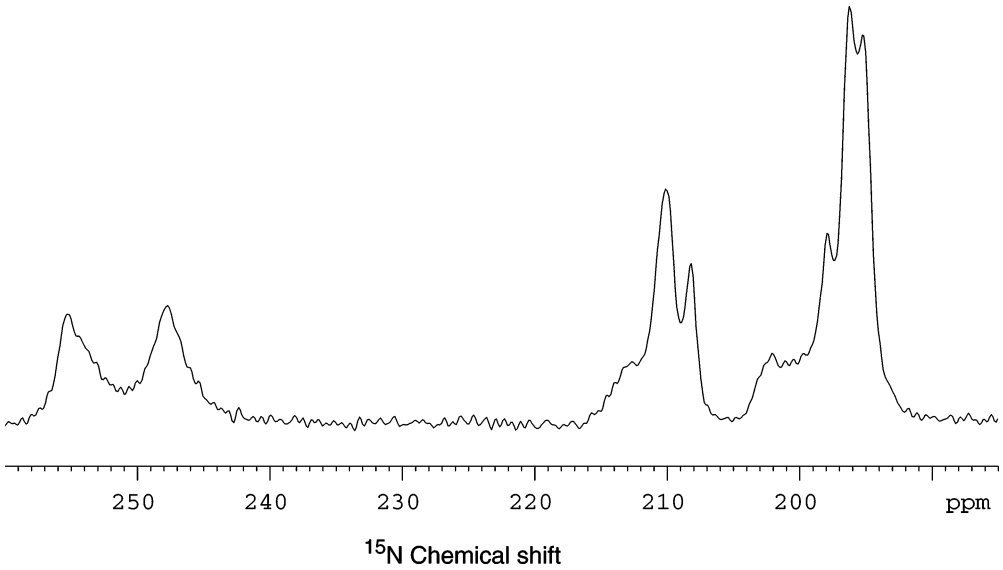

Figure 5. 1-D CP/MAS ^{15}N spectrum for the CH_2Cl_2-treated solid aggregate of uniformly ^{13}C- and ^{15}N-labeled (3^1R)-[*E*,*E*]BChl c_F in a magnetic field of 17.6 T. The MAS frequency and contact time were 12 kHz and 4 ms, respectively. Scans (14 400) were collected using a delay time of 2 s.

has been observed that a solid aggregate with an absorption band around 740 nm can be formed from both species upon drying the BChl *c*-CH_2Cl_2 solution.[33] The NMR data in this study suggest that the aggregation of (3^1R)-BChl *c* from a mixture of the antiparallel and transient dimers proceeds through different schemes: antiparallel stacking structure through the antiparallel dimer (Figure 8c) and a parallel stacking structure through a transient dimer form (Figure 8d). The antiparallel stacking structure is based on the ^{13}C chemical shifts for the type *A* solid species where upfield shift was observed only around ring I.

In this study, a solid species qualitatively corresponding to the component I in the native chlorosome could not be identified. Mizoguchi et al. suggested that addition of 3^1S-BChl *c* transforms the antiparallel stacking species to the parallel stacking structure.[28] A mixture of BChl *c* homologues might be necessary to form the component I structure. In a previous study, we had measured the X-ray diffraction powder for the CH_2Cl_2-treated solid aggregates of 3^1R-BChl *c* and the hexane-treated solid aggregates of a mixture of 3^1R- and 3^1S-bacteriochlorophylide (BChlide) *c* with the farnesyl group replaced by a methyl group. Both the aggregates showed two diffractions

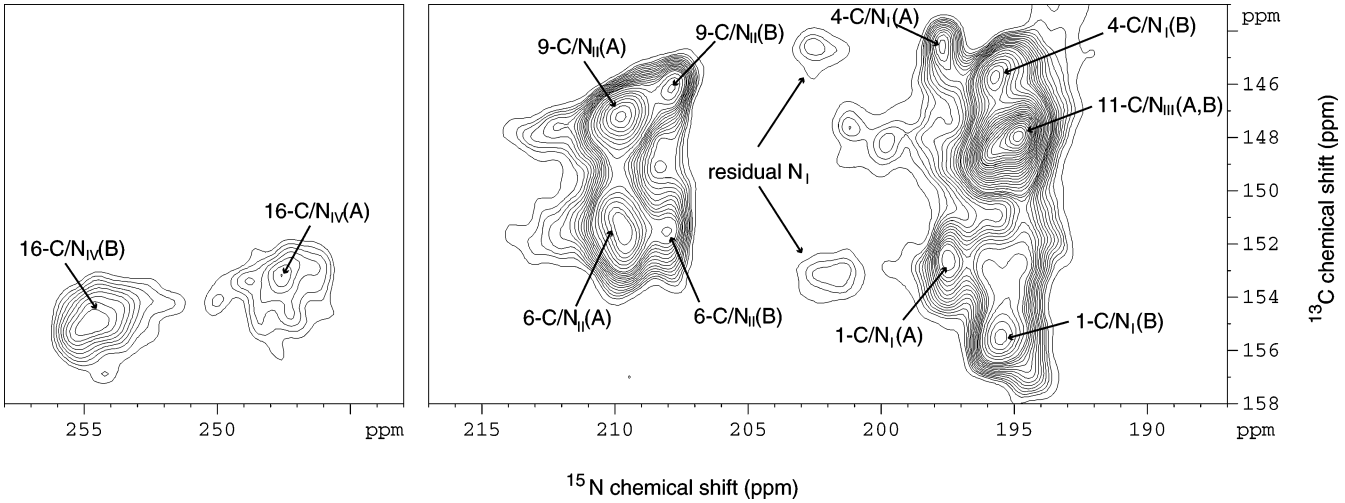

Figure 6. Contour plot of a 2-D heteonuclear $^{15}N-^{13}C$ correlation spectrum collected from the CH_2Cl_2-treated solid aggregate of uniformly ^{13}C- and ^{15}N-labeled (3^1*R*)-[*E*,*E*]BChl c_F. The data were recorded in a magnetic field of 17.6 T. The MAS frequency was 12 kHz, and the contact times for $^1H-^{13}C$ and $^{15}N-^{13}C$ polarization transfer were 2 and 5.1 ms, respectively. The numbering in the plot corresponds with Figure 1. The cross peaks labeled with A and B are the correlations linked with the networks A and B of carbon, respectively.

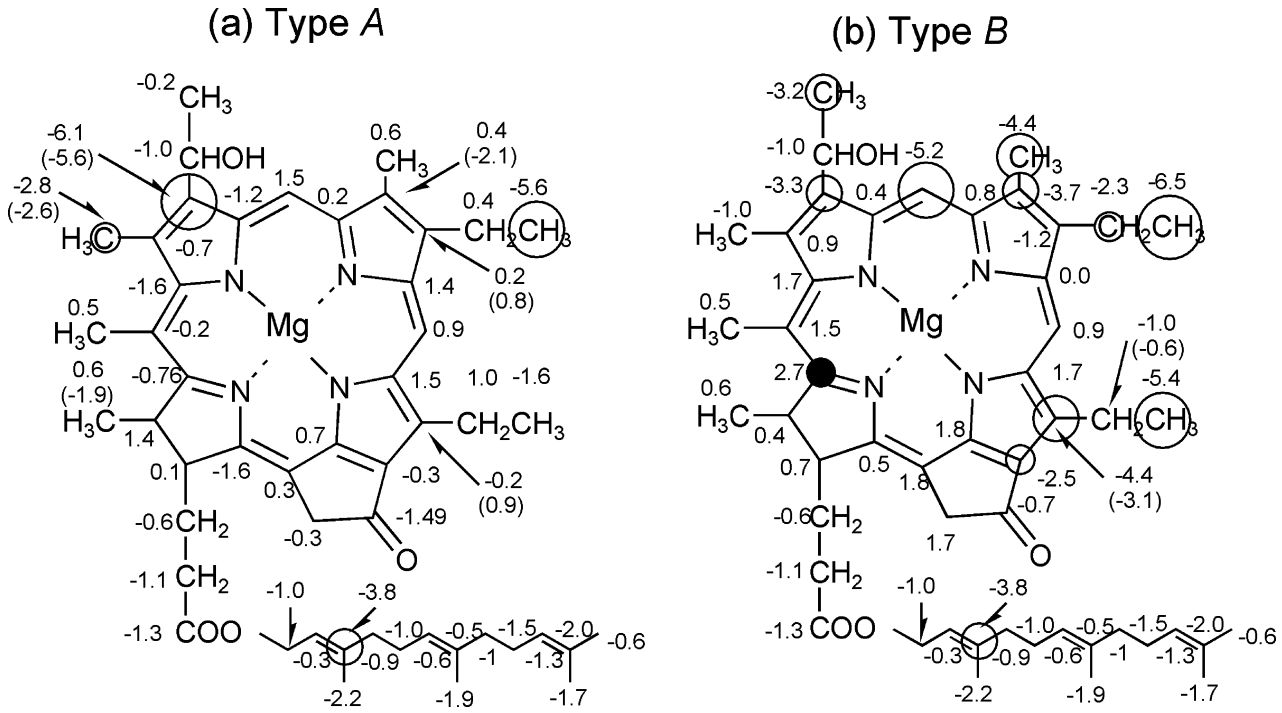

Figure 7. Schematic map showing the ^{13}C chemical shift difference, $\Delta\delta = \delta_{solid} - \delta_{monomer}$, for the type A (a) and B (b) of (3^1*R*)-[*E*,*E*]BChl c_F in the CH_2Cl_2-treated solid aggregate. All values were obtained using Table 1. The ^{13}C chemical shifts of monomeric (3^1*R*)-[*E*,*E*]BChl c_F are collected in a mixture of $CDCl_3$ and CD_3OD (v/v 1:9).[13] The carbons with the $\Delta\delta > \pm 2.0$ ppm are marked with a circle in the map. Open and closed circles correspond with negative and positive $\Delta\delta$, respectively. The sizes of the circles reflect the magnitude of the $\Delta\delta$.

at 13 and 18 Å, but the integrated area for the 18-Å band was much lower than that of the 13-Å band in the diffraction spectrum of the 3^1*R*/*S*- BChlide *c* aggregates, while both the band areas were almost comparable in the CH_2Cl_2-treated 3^1*R*-BChl *c* aggregates. Considering that the dimension between the two 13^1-C keto groups in an antiparallel dimer is approximately 18 Å, the diffractions at 13 and 18 Å might be derived from the parallel stacking structure (the type B solid species) and the antiparallel stacking structure (the type A solid species), respectively. In the $^{13}C-^{13}C$ correlation spectra, most carbon sites shows two chemical shift components with approximately equal intensities. The equal intensity of the carbon resonances and the X-ray diffraction bands suggests that the type A and B solid species are formed at a ratio of 1:1 in the CH_2Cl_2-treated 3^1*R*-BChl *c* aggregates.

The ^{15}N chemical shifts are assigned in this study from 1-D ^{15}N and 2-D heteronuclear $^{15}N-^{13}C$ correlation experiments. To our knowledge, these data represent the first observation of solid ^{15}N NMR signals detected from BChl *c* solid aggregates. N_I, N_{II}, and N_{IV} show at least two resonances, which is consistent with the suggestion from the ^{13}C NMR result that two different aggregated forms of BChl *c* (types A and B) coexist in the CH_2Cl_2-treated sample. Recently, ^{15}N NMR spectra have been measured for BChl *c* in methanol and in CCl_4, and ^{15}N chemical shifts have been assigned for a monomer state and an antiparallel dimer with a piggy-back conformation.[22] The

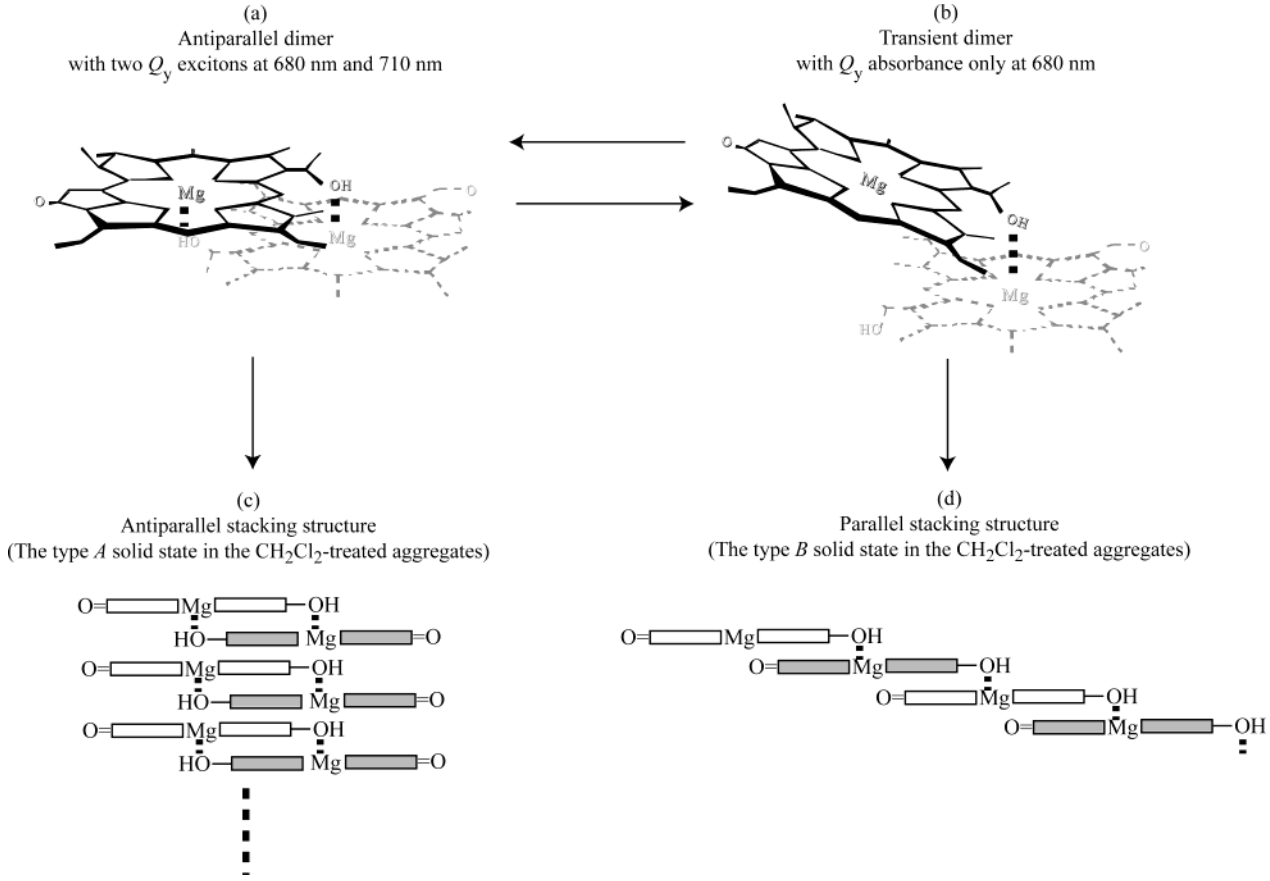

Figure 8. Schematic depiction of aggregation behavior. Aggregation of the antiparallel dimer (a) and the transient dimer (b) has been reported in refs 22 and 23. The antiparallel stacking structure (c) corresponds to the type-A solid species in the CH_2Cl_2-treated (3^1R)-[*E*,*E*]BChl c_F solid aggregates and is composed of the antiparallel dimer called closed dimer. The parallel stacking structure (d) corresponds to the type B solid species in the CH_2Cl_2-treated solid aggregates and is similar to the component II in native chlorosome as reported in ref 31.

TABLE 2: Assignments of ^{15}N Chemical Shifts of the (3^1R)-[*E*,*E*] BChl c_F in the Solid Aggregates Treated in CH_2Cl_2

	monomer (ppm)		antiparallel dimer (ppm)	solid aggregates from CH_2Cl_2[a] (ppm)			
position	acetone-d_6[b]	methanol-d_4[b]	CCl_4[c]	type A		type B	
N_I	197.35	199.36	198.44 199.72	197.7	(0.5)	195.7	(0.5)
N_{II}	209.71	212.58	209.04 211.87	209.8	(0.5)	208	(0.5)
N_{III}	193.65	196.64	195.50 195.69	194.8 (0.5)			
N_{IV}	248.51	250.66	245.44 249.56	247.5	(1.0)	254.5	(1.5)

[a] The estimated errors for the solid-state shifts are in parentheses. [b] Monomer shifts were determined from proton-decoupled ^{15}N spectra for uniformly ^{15}N-labeled (3^1R)-[*E*,*E*] BChl c_F in acetone-d_6 and methanol-d_4 at a concentration of 2 mM. [c] The chemical shifts for antiparallel dimer were measured in CCl_4 at a concentration of 2 mM.[22]

^{15}N chemical-shift dispersion is generally quite large, and ring-current effects are difficult to discriminate from the paramagnetic shielding effects on the nitrogen atom that reflect the details of the electronic environment and appear to predominate the ^{15}N chemical shift. Table 2 lists the ^{15}N chemical shifts of BChl *c* for the monomer states in acetone and in methanol, antiparallel dimer in CCl_4, and the CH_2Cl_2-treated solid aggregate. For N_I and N_{IV}, the chemical shifts in the type A solid state are comparable to the values for the antiparallel dimer, while the shifts for the type B species are different from the dimer state. This supports that the type-A solid species correspond with an antiparallel stacked form. It should be noted that the pronounced chemical shift difference of 7 ppm between the two signals assigned to N_{IV} is related to the large downfield shift of N_{IV} for the type B solid state. Ab initio quantum chemical calculations and solid state ^{15}N NMR studies on metal−tetraphenylporphyrin compounds indicate that ^{15}N chemical shifts tend to be determined by the metal−nitrogen separation.[46] Considering that the long ester chain is attached to only ring IV, the alignment of the ester long chain may induce some local steric strain to ring IV and affect the Mg−N_{IV} separation. Another ab initio study reveals that the population of N_{II} and N_{IV} π orbitals and δ bonds to Mg in ethyl-chlorophyllide *a* changes upon coordination of H_2O to the central Mg.[47] Athough the IR spectrum of the CH_2Cl_2-treated aggregate has suggested 5-coordinate Mg in the aggregate,[33] the N_{IV} for the methanol solution, where the Mg atom of BChl *c* is 6-coordinated,[7] has only a slight downfield shift of 2.15 ppm with respect to the 248.5-ppm resonance of N_{IV} in acetone with the 5-coordinate Mg atom (Table 2).[7]

In conclusion, we observed two sets of resonances for most of the carbons and nitrogens by 2-D homonuclear and hetero-

nuclear dipolar correlation NMR measurements in an ultrahigh magnetic field of 17.6 T, revealing two distinct different solid states in the CH_2Cl_2-treated (3^1R)-[*E*,*E*]BChl c_F solid aggregate. The chemical shifts of ^{13}C and ^{15}N in the type A solid state are different from those of the aggregates found in the chlorosomes. They resemble the antiparallel dimer in solution. The signal patterns suggest that (3^1R)-[*E*,*E*]BChl c_F forms two types of solid species through a different scheme, that is, the antiparallel stacking structure formed through the antiparallel dimer called close dimer and the parallel stacking structure through the transient dimer called open dimer. The formation of the stable close dimer can leads to the formation of non-native antiparallel stacking structure. Recent thermodynamics research demonstrates that (3^1S)-BChl *c* destabilizes the stable close dimer fromed by (3^1R)-[*E*,*E*]BChl *c*,[48] suggesting that in vivo (3^1S)-BChl *c* functions as an accelerator to convert the closed dimer to an open dimer. This indicates that the self-assembly of BChl *c* can be controlled by the chirality at the 3^1-position.

Acknowledgment. The authors would like to thank Kees Erkelens and Fons Lefeber for assistance during various stages of the NMR measurements and are grateful to Taku Kurisaki and Ryoichi Seki for the preparation of the BChl *c* sample. This work has been supported by a JSPS research fellowship for young scientists and JSPS postdoctoral fellowship for research abroad to M.U. J.M. acknowledges a Casimir−Ziegler award from the Academies of Sciences in Amsterdam and Düsseldorf. H.J.M.dG. is a recipient of a PIONIER award of the Chemical Sciences section of The Netherlands Organization for Scientific Research. The ultrahigh field equipment was financed in part by the commission of the European communities (BIO4-CT97-2101).

References and Notes

(1) Blankenship, R. E.; Olson, J. M.; Miller M. In *Anoxygenic Photosynthetic Bacteria*; Blankenship, R. E., Madigan, M. T., Bauer, C. E., Eds.; Kluwer Academic Publishers: Dordrecht, 1995; p 399.

(2) Staehelin, L. A.; Golecki, J. R.; Fuller, R. C.; Drew, G. *Arch. Mikrobiol.* **1978**, *119*, 269.

(3) Staehelin, L. A.; Golecki, J. R.; Drew, G. *Biochim. Biophys. Acta* **1980**, *589*, 30.

(4) Constantopoulos, G.; Bloch, K. *J. Bacteriol.* **1967**, *93*, 1788.

(5) Cruden, D. L.; Stanier, R. Y. *Arch. Microbiol.* **1970**, *72*, 115.

(6) Blankenship, R. E.; Brune, D. C.; Freeman, J. M.; Trost, J. T.; King, G. H.; McManus, J. H.; Nozawa, T.; Wittmershaus B. P. In *Green Photosynthetic Bacteria*; Olson, J. M., Ormerod, J. G., Amesz, J., Stackebrandt, E., Trüper, H. G., Eds.; Plenum Press: New York, 1988; p 57.

(7) Umetsu, M.; Wang, Z.-Y.; Kobayashi, M.; Nozawa, T. *Biochim. Biophys. Acta* **1999**, *1410*, 19.

(8) Wechsler, T.; Suter, F.; Fuller, R. C.; Zuber, H. *FEBS Lett.* **1985**, *181*, 173.

(9) Lehmann, R. P.; Brunishola, R. A.; Zuber, H. *FEBS Lett.* **1994**, *342*, 319.

(10) Lehmann, R. P.; Brunishola, R. A.; Zuber, H. *Photosynth. Res.* **1994**, *41*, 165.

(11) Olson, J. M.; Gerola, P. D.; van Brakel, G. H.; Meiburg, R. F.; Vasmel, H. In *Antennas and Reaction Centers of Photosynthetic Bacteria*, *Springer Ser. Chem. Phys. 42*; Michel-Beyerle, M. E., Ed.; Springer: Berlin, 1985; p 67.

(12) Brune, D. C.; Nozawa, T.; Blankenship, R. E. *Biochemistry* **1987**, *26*, 8644.

(13) Balaban, T. S.; Holzwarth, A. R.; Schaffner, K.; Boender, G. J.; de Groot, H. J. M. *Biochemistry* **1995**, *34*, 15259.

(14) Hirota, M.; Moriyama, T.; Shimada, K.; Miller, M.; Olson, J. M.; Matsuura, K. *Biochim. Biophys. Acta* **1992**, *1099*, 271.

(15) Miller, M.; Gillbro, T.; Olson, J. M. *Photochem. Photobiol.* **1993**, *57*, 98.

(16) van Noort, P. I.; Zhu, Y.; LoBrutto, R.; Blankenship, R. E. *Biophys. J.* **1997**, *72*, 316.

(17) Uehara, K.; Mimuro, M.; Ozaki, Y.; Olson, J. M. *Photosynth. Res.* **1994**, *41*, 235.

(18) Olson, J. M.; Pedersen, J. P. *Photosynth. Res.* **1990**, *25*, 25.

(19) Olson, J. M.; Cox, R. P. *Photosynth. Res.* **1991**, *30*, 35.

(20) Wang, Z.-Y.; Umetsu, M.; Yoza, K.; Kobayashi, M.; Imai, M.; Matsushita, Y.; Niimura, N.; Nozawa, T. *Biochim. Biophys. Acta* **1997**, *1320*, 73.

(21) Wang, Z.-Y.; Umetsu, M.; Kobayashi, M.; Nozawa, T. *J. Phys. Chem. B* **1999**, *103*, 3742.

(22) Wang, Z.-Y.; Umetsu, M.; Kobayashi, M.; Nozawa, T. *J. Am. Chem. Soc.* **1999**, *121*, 9363.

(23) Umetsu, M.; Seki, R.; Wang, Z.-Y.; Kumagai, I.; Nozawa, T. *J. Phys. Chem. B* **2002**, 3987.

(24) Chiefari, J.; Griebenow, K.; Griebenow, N.; Balaban, T. S.; Holzwarth, A. R.; Schaffner, K. *J. Phys. Chem.* **1995**, *99*, 1357.

(25) Mizoguchi, T.; Matsuura, K.; Shimada, K.; Koyama, K. *Chem. Phys. Lett.* **1996**, *260*, 153.

(26) Mizoguchi, T.; Sakamoto, S.; Koyama, K.; Ogura, K.; Inagaki, F. *Photochem. Photobiol.* **1998**, *67*, 239.

(27) Balaban, T. S.; Tamiaki, H.; Holzwarth, A. R.; Schaffiner, K. *J. Phys. Chem. B* **1997**, *101*, 3424.

(28) Mizoguchi, T.; Hara, K.; Nagae, H.; Koyama, Y. *Photochem. Photobiol.* **2000**, *71*, 596.

(29) Nozawa, T.; Ohtomo, K.; Suzuki, M.; Nakagawa, H.; Shikama, Y.; Konami, H.; Wang, Z.-Y. *Photosynth. Res.* **1994**, *41*, 211.

(30) van Rossum, B. J.; Boender, G. J.; Mulder, F. M.; Raap, J.; Balaban, T. S.; Holzwarth, A. R.; Schaffner, K.; Prytulla, S.; Oschkinat, H.; de Groot, H. J. M. *Spectrochim. Acta A* **1998**, *54*, 1167.

(31) van Rossum, B. J.; Steensgaard, D. B.; Mulder, F. M.; Boender, G. J.; Schaffner, K.; Holzwarth, A. R.; de Groot, H. J. M. *Biochemistry* **2001**, *40*, 1587.

(32) Smith, K. M.; Craig, G. W.; Kehres, L. A.; Pfennig, N. *J. Chromatogr.* **1983**, *281*, 209.

(33) Umetsu, M.; Wang, Z.-Y.; Zhang, J.; Ishii, T.; Uehara, K.; Inoko, Y.; Kobayashi, M.; Nozawa, T. *Photosynth. Res.* **1999**, *60*, 229.

(34) Wahlund, T. M.; Woese, C. R.; Castenholz, R. W.; Madigan, M. T. *Arch. Microbiol.* **1991**, *156*, 81.

(35) Bennett, A. E.; Rienstra, C. M.; Auger, M.; Lakshmi, K. V. *J. Chem. Phys.* **1995**, *103*, 6951.

(36) Metz, G.; Wu, X.; Smith, S. O. *J. Magn. Reson. A* **1994**, *110*, 219.

(37) Bennett, A. E.; Ok, J. H.; Griffin, R. G.; Vega, S. *J. Chem. Phys.* **1992**, *96*, 8624.

(38) Bloembergen, N. *Physica* **1949**, *15*, 386.

(39) van Rossum, B. J.; Förster, H.; de Groot, H. J. M. *J. Magn. Reson.* **1997**, *124*, 516.

(40) Baldus, M.; Petkova, A. T.; Herzfeld, J.; Griffin, R. G. *Mol. Phys.* **1998**, *95*, 1197.

(41) Egorova-Zachernyuk, T. A.; Hollander, J.; Fraser, N.; Gast, P.; Hoff, A. J.; Cogdell, R.; de Groot, H. J. M.; Baldus, M. *J. Biomol. NMR* **2001**, *19*, 243.

(42) Pauli, J.; Baldus, M.; van Rossum, B. J.; de Groot, H. J. M.; Oschkinat, H. *Chem. Biochem.* **2001**, *2*, 272.

(43) Abraham, R. J.; Smith, K. M. *J. Am. Chem. Soc.* **1983**, *105*, 5734.

(44) Boender, G. J.; Raap, J.; Prytulla, S.; Oschkinat, H.; de Groot, H. M. J. *Chem. Phys. Lett.* **1995**, *237*, 502.

(45) Mizoguchi, T.; Ogura, K.; Inagaki, F.; Koyama, Y. *Biospectroscopy* **1999**, *5*, 63.

(46) Strohmeier, M.; Orendt, A. M.; Facelli, J. C.; Solum, M. S.; Pugmire, R. J.; Parry, R. W.; Grant, D. M. *J. Am. Chem. Soc.* **1997**, *119*, 7114.

(47) Spangler, D. G.; Maggiora, M.; Shipman, L. L.; Christoffersen, R. E. *J. Am. Chem. Soc.* **1977**, *99*, 7478.

(48) Umetsu, M.; Seki, R.; Kadota, T.; Wang, Z.-Y.; Adschiri, T.; Nozawa, T. *J. Phys. Chem. B* **2003**, *107*, 9876.